8

Hydro-stratigraphic study of the Hydrogeological Experimental Site of Poitiers, France

T. Gaillard

Objectif and method

The Hydrogeological Experimental Site (HES), located near Poitiers (France), was originally established to investigate the role of fracturing in Middle Jurassic limestones. The supra-Toarcian aquifer has been extensively characterized through surface geophysics (Mari et al., 2009), borehole geophysical logging (Mari et al., 2020; Moreau et al., 2026), and numerous downhole investigations conducted by the University of Poitiers (Delay et al., 2004).

Early studies demonstrated the absence of major vertical structures such as faults or open vertical fractures. However, the presence of discontinuous sub-horizontal porous horizons has been clearly documented (Bourbiaux et al., 2007; Audouin et al., 2008; Mari et al., 2009; Bodin et al., 2022; Mari et al., 2024). In this paper, these planar features are reinterpreted within the framework of the regional stratigraphic context (Gabilly, 1978; Mourier et al., 1986; Gaillard et al., 2024) and by

DOI: https://doi.org/10.1051/978-2-7598-3934-6.c008

comparison with geological outcrops in the Clain Valley (Branger et al., 2026). Dating of sedimentation across the Poitou Threshold (Fig. 1) remains difficult, as ammonite occurrences are rare and largely restricted to the base of the depositional sequence (Gabilly, 1978, p. 150). Consequently, stratigraphic interpretation relies primarily on the identification of erosional surfaces (Gabilly et al., 1985), bed thickness, fossil assemblages, and established regional reference sections (Gabilly, 1978; Mourier et al., 1986).

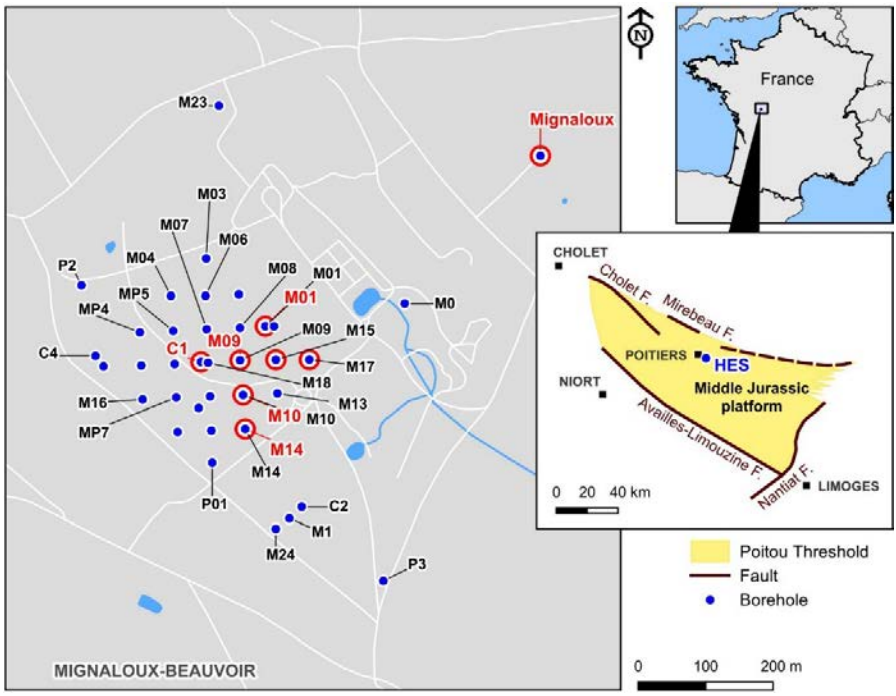

Figure 1 *The hydrological experimental site and borehole locations (Poitiers University document).*

This study is based on the analysis of two continuous cores (C1 and C2) and high-resolution borehole optical imagery (OPtical TeleView - OPTV). Figure 1 shows the location of the HES, the core drillings, and the Mignaloux borehole described by Mourier (1983).

Aquifer stratigraphy of the HES

Stratigraphic context

The reference stratigraphy for the supra-Toarcian aquifer is derived from the works of Gabilly (1978), Benvel (1978), and Mourier (1986). For further details about

the Bajocian, refer to Branger et al. (2026). The discontinuities (D) are numbered according to Gabilly et al (1985).

The Aalenian stage is subdivided into three main terms with reference to ammonite zones (base to top):

a) laminated marly limestones (*Opalinum* Biozone, 4–5 m),
b) siliceous (cherty) formation (*Murchisonae* Biozone, 8–10 m),
c) bioclastic and oolitic limestones (*Bradfordensis* and *Concavum* Biozones, 9–14 m), often partially dolomitized and locally displaying cavernous textures (c′ unit).

A regional discontinuity (D5bis) separates the *Opalinum* and *Murchisonae* Biozones, while discontinuities D6 and D7 mark the base and top of the *Concavum* interval.

The Bajocian comprises:

d) decimetric limestone beds with Serpulid fossils (*Ovalis* Biozone, 1–2 m),
e) bioclastic and pelletal limestones (*Laeviuscula* Biozone, 7–8 m),
f) white oolitic limestones (top of *Laeviuscula*, 2–4 m),
g) limestone beds of the *Propinquans* and *Humphriesianum* Biozones (9–10 m), topped by h) a crinoid-rich horizon,
h) bioturbated limestones referred to as the burrowed limestones "Assise à terriers" (*Garantiana* Biozone, 5–6 m), and
i) fine-grained gravelly limestones with flint nodules (*Parkinsoni* Biozone, 23–25 m).

Discontinuities are identified at the top of the *Laeviuscula* zone (D7bis) and at the base and top of the *Garantiana* interval (D8 and D8bis, respectively).

The Bathonian is more difficult to interpret due to gaps in biostratigraphic markers. Bathonian limestones lie above discontinuity D9. Gabilly (1978) subdivided this interval into:

k) ctenostreon beds (possibly *Zigzag* Biozone?, 2–3 m),
l) siliceous, bioclastic and pelletal limestones (15–16 m),
m) bioturbated limestones (7 m).

The overlying Callovian is easily recognizable due to its micropackstone texture and chalky appearance.

Data available

The borehole drilled during Mourier's thesis (1983), near the HES, identified key marker horizons (notably the oolitic limestone of the *Concavum* Biozone and the crinoidal bed atop the *Humphriesianum* interval). Stratigraphic details for the supra-Toarcian aquifer were further refined using two cored boreholes (C1 and C2) described by the French Petroleum Institute (Gaumet et al., 2004). These cores made it possible to characterize the depositional facies (mudstone, packstone,

grainstone) and provided a preliminary sequence stratigraphy. However, erosional surfaces were poorly sampled and often absent in the cores.

To address this shortcoming, borehole optical imagery was analysed for the first time and presented at the "Journées Scientifiques de l'AGAP-Qualité" at the University of Poitiers (Gaillard et al., 2024). OPTV logs offer high-resolution imaging of bedding surfaces and discontinuities, enhancing the identification of sequence boundaries described on the Poitou Threshold (Gabilly, 1978; Gabilly et al., 1985; Gaillard et al., 2024; Branger et al., 2026).

Initial OPTV analyses were focused on boreholes with minimal karstification and long open-hole sections (M01, M09, M10, M14, M15, M17). Subsequent analyses targeted boreholes extensively studied through geophysics and hydrogeological testing. Additional data include resistivity and natural gamma-ray logs.

Table 1 *List of open holes and drilling cores studied.*

Borehole	X_RGF93	Y_RGF93	Z NGF	Depth of top OH in m	Depth of bottom OH	OH length in m
C1	501299.97	6609513.918	125.36	23.8	129.7	129.70
C2	501449.316	6609299.466	123.12	/	/	
C3	501359.815	6609493.411	125.65	/	/	
M01	501395.377	6609566.963	124.95	20.4	125.7	105.3
M09	501357.926	6609516.374	125.48	33.0	121.0	88.0
M10	501362.346	6609464.802	125.98	20.0	117.0	97.0
M14	501308.442	6609562.542	124.71	23.4	120.0	96.6
M15(b)	501357.803	6609564.507	124.89	23.5	124.5	101.0
M17	501460.577	6609517.356	124.05	23.0	128.0	105.0

RGF93: French geodesic system in meters; NGF: meter above sea level (masl) in the French elevation system; OH: open hole section.

A summary of the results is proposed to properly constrain the HES stratigraphy with reference to the regional geological context. Figure 1 shows the locations of boreholes and core drilling.

Lithostratigraphy of the HES

The Callovian/Bathonian boundary can be observed in core logs. The Callovian limestone is a chalky, porous micropackstone to packstone containing peloids. On the OPTV log, discontinuity D11 is clearly visible in borehole M01 at a depth of 23.15 m and 23.02 m in M10, appearing as a sharp planar erosion surface (Fig. 2). A comparable surface is identified at 23.17 m depth in the PZ6 located between MP7 and M21.

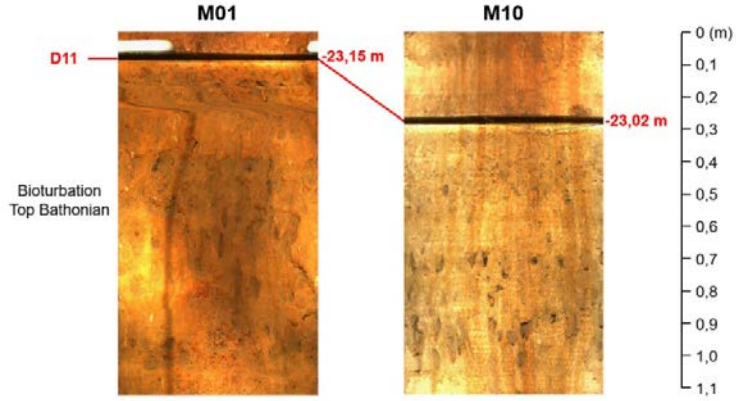

Figure 2 *Bathonian / Callovian transition with D11 discontinuity.*

The Middle Bathonian is characterized by bioturbated limestone with basal chert layers. The formation thickness exceeds 2.20 m in M01 and 3.30 m in M10. At the Poitiers cliff outcrop, a comparable unit was described as gravelly and oolitic limestone containing *Procerites sp*. (Gabilly, 1978, p. 150).

The Bathonian flinty limestone corresponds to a micrograinstone facies, previously described as sub-oolitic limestone by Gabilly (1978). Two distinct chert bands are observed at the top of this formation, clearly identifiable in boreholes M15 and M10. This double chert band is characteristic of the "Assise à silextite" (flint band) described by Mourier (1986) and Gabilly (1978).

A significant change in sedimentation occurs above the 42 m depth, where very fine-grained limestones overlie a bioturbated interval between 42 and 45 m depth (noted in M10, M14, and M15). This lithological transition is interpreted as marking the Bajocian–Bathonian boundary (Fig. 3). A *Ctenostreon* fossil was recovered from the inclined borehole C4 at a depth of 66.25 m. Considering the borehole's

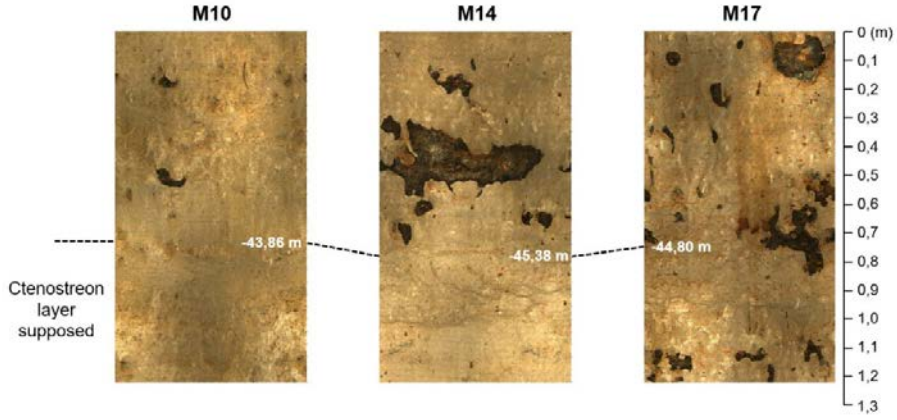

Figure 3 *Bajocian – Bathonian transition (D9 discontinuity).*

inclination (26°), the true vertical depth of the fossil is calculated at approximately 42 m. This finding supports the identification of the Bajocian–Bathonian boundary at 42 m, previously inferred from OPTV data based on the presence of two strongly bioturbated layers in boreholes M10, M14, and M15 (Fig. 3).

The D9 discontinuity, which defines the base of the Bathonian, appears subtly on OPTV images at depths of 45.60 m in M14, 45.10 m in M15 (visible at a bedding joint), and 45.02 m in M17.

A flinty limestone unit is consistently observed below the planar erosion surface identified as D9. This unit is characterized by intense bioturbation around a depth of 50 m and the presence of distinctive chert (flint) bands that can be correlated between boreholes using OPTV data. A wavy erosional surface, highlighted by a concentration of bivalve shells, marks the top of the first depositional sequence of the *Parkinsoni* Biozone. This surface is observed at the following depths: M01 (61.77 m), M10 (62.49 m), M14 (62.35 m), M15 (63.60 m), and M17 (59.12 m) (Fig. 4).

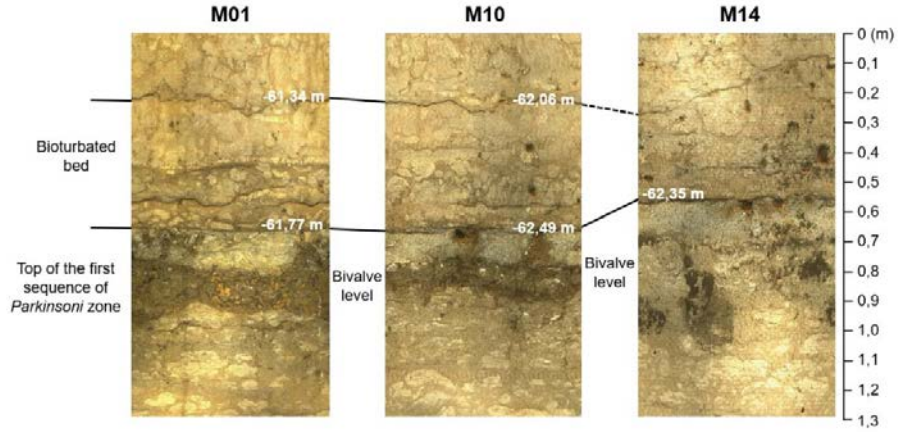

Figure 4 *Top of the first "Parkinsoni" sequence.*

A major planar erosional surface, underlain by a clay-rich horizon, defines the top of the bioturbated formation traditionally referred to as the "Assise à terriers" (Fig. 5). This key stratigraphic surface is clearly identified in several boreholes: M01 (64.81 m), M02 (65.48 m), M10 (65.48 m), M14 (65.31 m), M15 (63.60m) and M17 (62.25 m). It is interpreted as corresponding to the regional D8bis discontinuity.

A bioclastic horizon, associated with the base of this formation, is recorded at 67.00 m in the C1 core and identified at 66.42 m in M01 and 67.05 m in M10. The base of this unit is marked by a wavy erosional surface overlying a 15 cm thick bed rich in *Trichites* sections (Mollusca). This surface is well expressed across several HES boreholes: M01 (72.15 m depth), M10 (71.99 m), M14 (71.13 m), M15 (72.00 m), and inferred at 70.63 m in M17. This erosional boundary is interpreted as the D8 discontinuity (Fig. 6).

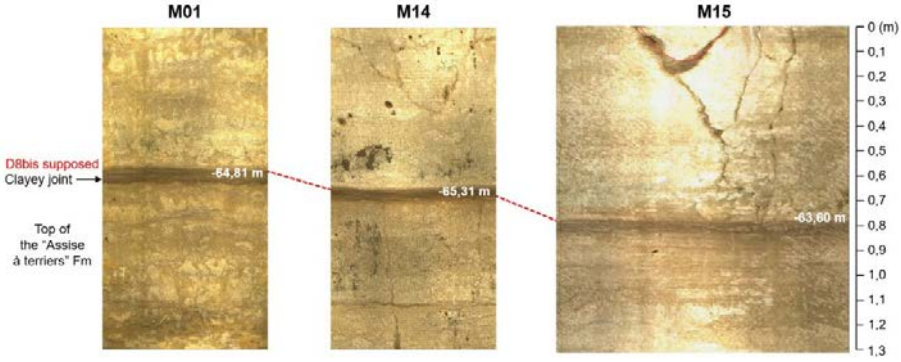

Figure 5 *Clayey joint at the top of the "Assise à terriers" Formation (D8bis discontinuity).*

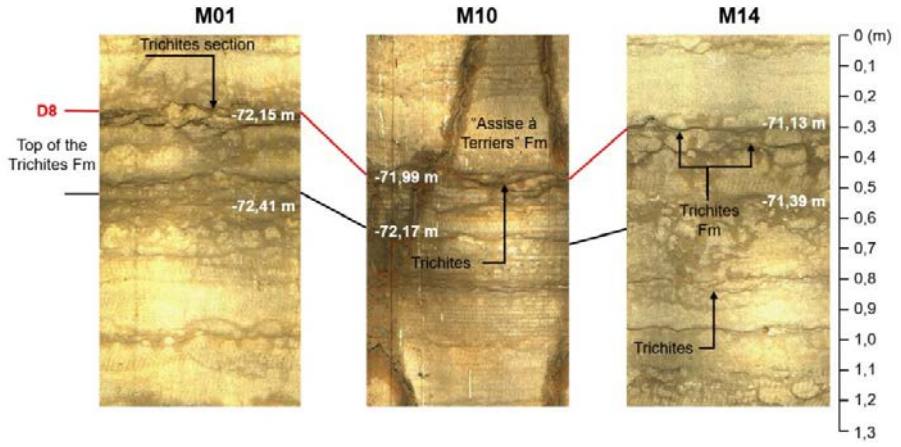

Figure 6 *Transition between* Trichites *formation and the "Assise à terriers" formation.*

The *Trichites* Limestone Formation is composed of pluricentimetric beds of packstone, each capped by a bioturbated horizon rich in Trichites sections. Based on the C1 core description, the formation begins with grain-supported lamination, producing a distinctive "snake-skin" facies on OPTV imagery (Gaillard et al., 2024). The initial stratum of the Trichites Formation is approximately 30 cm thick and is consistently bounded at the top by a clayey joint visible on all OPTV logs.

The *Trichites* Formation directly overlies the Oolitic limestone Unit corresponding to the upper *Laeviuscula* Biozone. This oolitic interval is readily identifiable in core material. On OPTV logs, the Oolitic limestone appears as a white level composed of 3 grainstone strata that are about 1 m thick each. The base of this unit is marked by a discontinuous black clay observed at the following depths: M01 (84.35 m), M09 (84.45 m), M10 (85.37 m), M14 (84.97 m), and M17 (81.87 m). The upper sequence boundary corresponds to the contact with a 50 cm-thick bed identified on all OPTV logs. The contact between the 50 cm thick bed and the Trichites Formation is equivalent to the D7bis discontinuity.

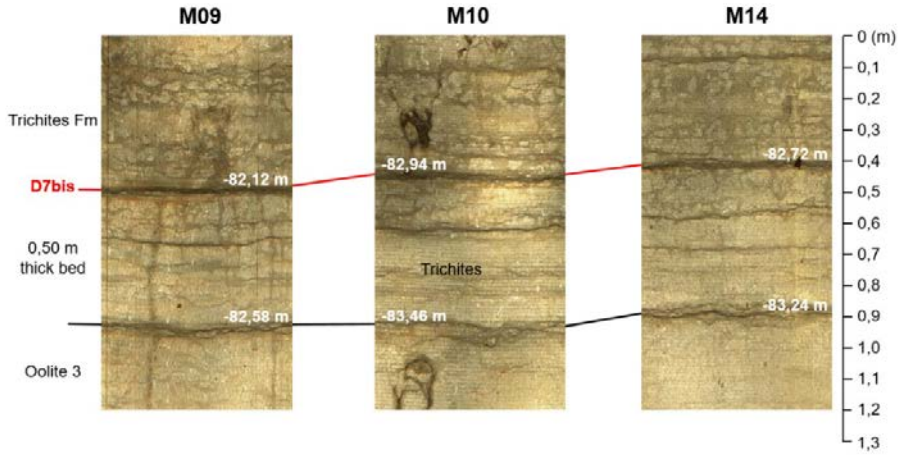

(a) D7bis discontinuity

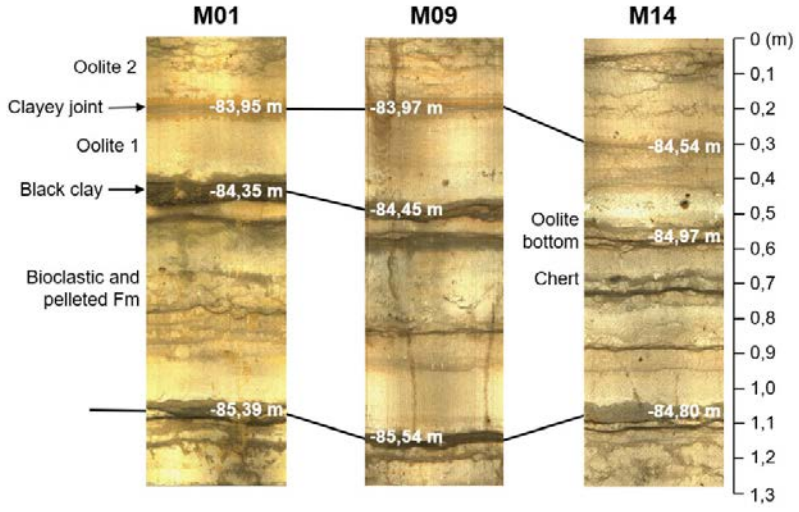

(b) Lower sequence boundary (Oolitic unit/Formation)

Figure 7 *Sequence boundaries of the Oolite unit.*

Beneath the Oolitic Formation, the limestone is a bioclastic and peloidal facies characteristic of the *Laeviuscula* Biozone. A vuggy interval of black dolomite, likely related to pyrite oxidation contained in black clay, is clearly visible within the upper dolomitized section of the oolitic facies. Similar vuggy textures are observed at the Passelourdin cliff, located approximately 2 km south of the HES (Branger et al., 2026).

At the base of this unit, two distinctive beds are consistently identified across all OPTV logs. The upper bed, approximately 0.60 m thick, is bounded by two pronounced joints and is rich in crinoids and bivalves. The lower bed, ranging

from 0.60 to 0.80 m thick, underlies a hardground surface associated with a bivalve-rich horizon. The upper bed is correlated with the *Galeolaria socialis* (serpulidae) bed described by Gabilly (1978) and is interpreted as marking the base of the *Laeviuscula* Biozone (Fig. 8). Based on this interpretation, the *Laeviuscula* Zone begins at 95.59 m (M01), 95,92 m (M09), 96.61 m (M10), and 96.26 m (M14). The bioclastic horizon beneath the hardground forms part of a 0.80 m thick fossiliferous bed, whose basal contact is a planar to undulating erosional surface. This surface is interpreted as the Aalenian–Bajocian unconformity (D7) and is observed at 96.41 m (M01), 97.52 m (M10), and 97.20 m (M14). The lower stratum is tentatively assigned to the *Ovalis* Biozone (Gabilly, 1978, p. 148) with the identification of a *Sonninidae* in the Saint Benoit cliff by Patrick Branger, 4 kilometers south of the HES. D7 discontinuity delimits a vacuolated texture interval with a dark hue, referred to as the Middle Dolomitized Zone.

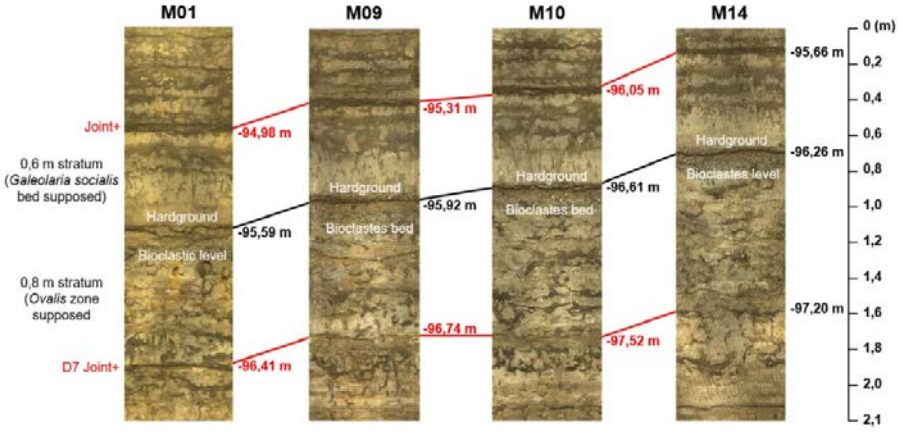

Figure 8 *Bajocian lower boundary.*

Below the D7 discontinuity, a packstone unit can be correlated with the oolitic and oncolitic facies of the *Concavum* Biozone (Mourier, 1986, p. 13). At its base, chert nodules and bands following bedding planes are present, particularly at 98.56 m (M14). These cherts, typically 20–30 cm thick, are attributed to the *Murchisonae* Biozone of the Aalenian, though their stratigraphic value is limited due to their occurrence across multiple Biozones (Benvel, 1978; Mourier, 1986).

Two hardgrounds are recognized at the base of this formation, at 105.86 m (M10) and 105.21 m (M14), and are cautiously correlated—due to dolomitization effects—with the D6bis discontinuity. Another hardground, observed at 110.15 m (M10) and 110.85 m (M14), marks the top of a decimetric-bedded limestone unit. The base of this unit is poorly defined on OPTV logs because of intense dolomitization (Lower dolomitized zone). This hardground is correlated with the D6 discontinuity.

A change in sedimentation is observed at 119.10 m (M14) and likely corresponds to the top of the Toarcian marls. In another OPTV borehole (M09), this boundary

occurs at 119.92 m, supporting the correlation. Above this surface, a bivalve-rich level—interpreted as the *Gryphaea beaumonti* bed—is recognized and considered to mark the base of the Aalenian.

Figure 9 presents a stratigraphic synthesis of the supra-Toarcian aquifer at the HES.

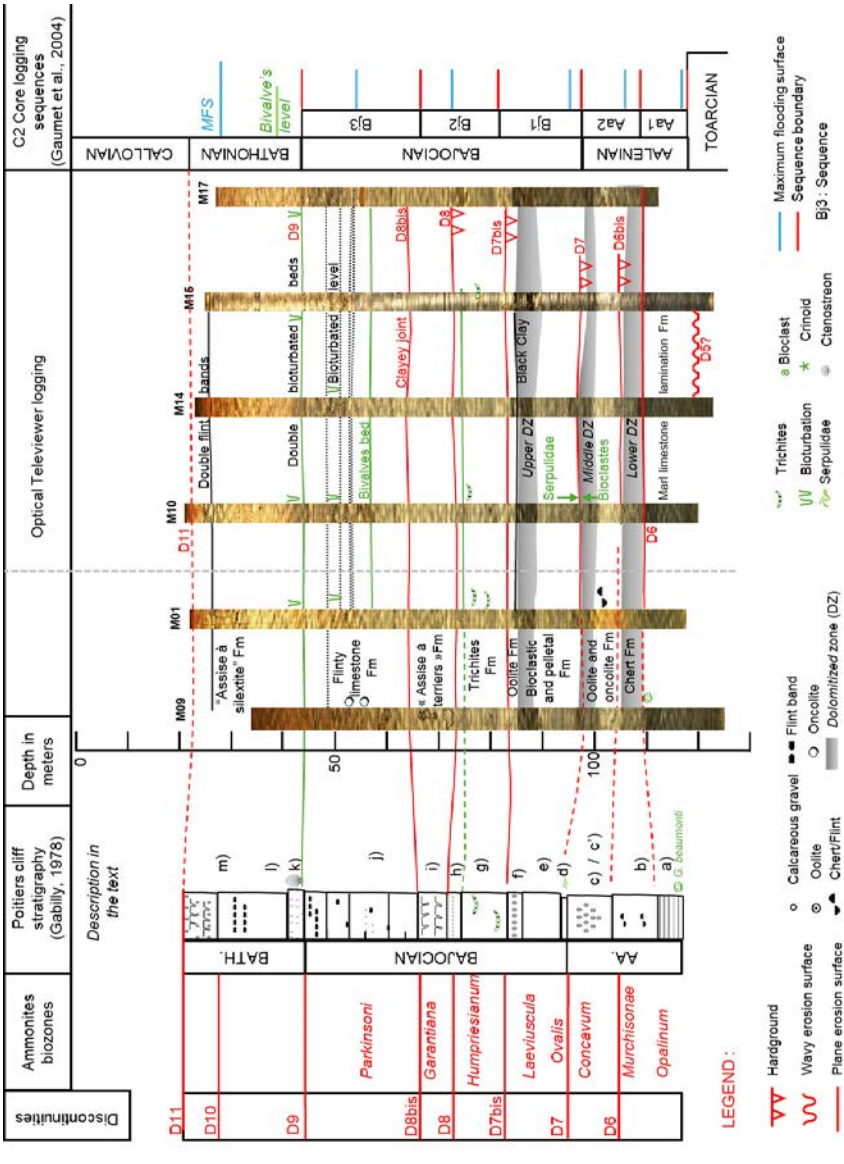

Figure 9 *Stratigraphical synthesis of HES boreholes.*

Occurrence ok karst

Fracture inventory

Audouin et al. (2008) identified a set of potentially productive fractures through the integration of heat-pulse flowmeter measurements and OPTV borehole imaging. While some of these features reveal the morphology of inclined fractures—as observed in borehole M07—most are interpreted as the result of collapse within karstified horizons and are more accurately described as sedimentary joints. Based on their analysis, the authors concluded that fewer than 3% of the identified fractures appear to be hydraulically conductive.

To verify and expand upon these conclusions, a comprehensive review of all OPTV logs of this study was conducted, focusing specifically on the identification of inclined and vertical fractures. These were systematically mapped across the boreholes to assess their spatial distribution and relationship to karstic voids. The results are compiled in Table 2, which lists the depths and apparent apertures of each feature. Only non-horizontal fractures (i.e., vertical and inclined) are included in this dataset; horizontal features, interpreted as bedding planes or sedimentary joints, were excluded from this classification.

Table 2 *Depth of fractures reported on OPTV logs.*

Boreholes	Fracture typology		
	Open	Filled by clay	Recrystallised
M01	0	1 38.67-39.80	0
M09			6 (36.71-37.70; 60.00-60.84; 66.53-70.13; 71.31-72.25; 72.52-73.73; 84.58-85.49)
M10	0	0	0
M14	1 73.25-73.60;	0	1 85.49-85.75
M15(b)	1 47.8-48.8	1 61.4-63.0	0
M17	0	0	1 (43.02-44.19)

The total length of all boreholes equals 593 m. Within these 593 meters, only 12 fractures are well identified, which gives a density of 0,02 fractures per meter. This ratio is largely due to M09, with 6 fractures identified. In general, reported fractures are located above the Oolite Formation of the *Laeviuscula* Biozone and are not present in Aalenian limestones. Only two of them are open and could provide water flow.

Stratigraphy versus seismic and acoustic data

Following earlier studies (Bourbiaux et al., 2007; Audouin et al., 2008), a 3D seismic survey was carried out (Mari & Porel, 2008; Mari, 2026) to obtain a volumetric image with extensive horizontal coverage. Structural interpretation revealed a nearly horizontal stratigraphy with a gentle westward dip of about one degree, confirming the absence of significant vertical tectonic displacements.

The 3D seismic volume was subsequently converted into a pseudo-velocity model, calibrated using acoustic velocity logs, and then into a pseudo-porosity model (Fig. 10; Mari et al., 2009; Delay et al., 2022). This seismic-derived porosity model highlighted three high-porosity—and presumably water-bearing—layers at depths of 35–40 m, 85–87 m, and 110–115 m, which were interpreted as karstic horizons. These porous levels are subhorizontal but laterally discontinuous across the HES study area.

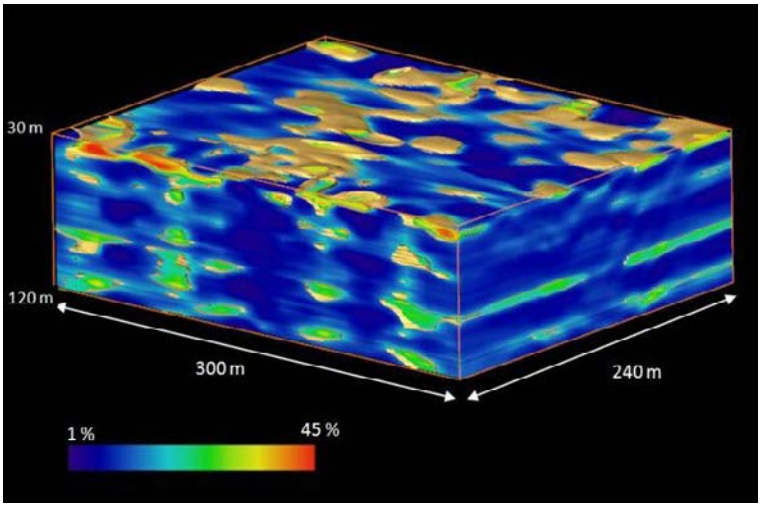

Figure 10 *3D Seismic porosity block in the 30–120 m depth interval. Modified after Mari et al. 2009, Delay et al., 2022.*

An integrated approach has since been developed to identify effective three-dimensional (3D) discrete karst conduit networks, constrained by tracer tests and geophysical data (3D seismic velocity block) (Bodin et al., 2022). The karstic horizons were independently confirmed through acoustic logging and borehole wall imaging with an Optical Televiewer (OPTV). In addition, a specific acoustic attribute, the Karstic Index, was introduced to identify karstic bodies (Fig. 11). However, owing to the relatively low vertical resolution of seismic data (meter scale) compared with borehole logs (centimeter to decimeter scale), some karstic features were detected only through borehole investigations.

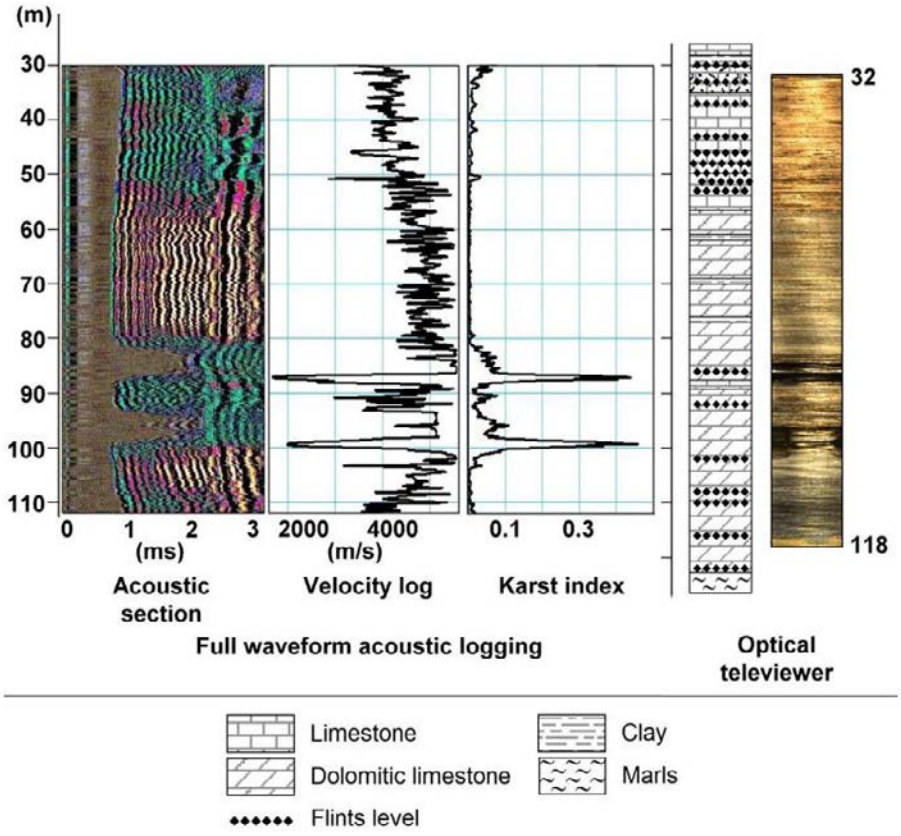

Figure 11 *Comparison of acoustic and optical wall imaging methods in borehole M20. From left to right: acoustic section, velocity log, karst index log, geological log, and optical wall imagery (OPTV).*

The uppermost porous horizon corresponds to bioturbated Bathonian limestones with bivalve assemblages, attributed to the "Assise à silextite" formation (flint band formation). This level covers the "banc à Ctenostreon," which marks the base of the Bathonian. This level is difficult to interpret using optical imagery, as most boreholes are cased down to 35 m depth. Only boreholes MP4, M17 and M22 reveal a more porous interval around 35 m. The intermediate porous interval, observed between 85 and 87 m depth, corresponds to the first dolomitized interval within the Oolitic Formation. It is characterized by centimetric vugs and coincides with the top of the "Bioclastic and Pelleted Formation," underlying the D7bis discontinuity. The coalescence of vugs may account for the formation of meter-scale cavities occasionally observed in optical televiewer images. The lowermost porous horizon is associated with the D6 discontinuity and corresponds to the Lower dolomitized zone.

For further details about seismic and acoustic methods, refer to Chapter 5 (Mari, 2026).

Stratigraphy versus borehole electrical methods

This stratigraphic framework has not yet been thoroughly correlated with borehole geophysical logging data, particularly natural gamma-ray (NGR) and resistivity logs (single point, short normal, and long normal). The main limitation lies in the difficulty of aligning the detailed stratigraphic interpretation with NGR signals, which generally provide low resolution in carbonate settings, and to a lesser extent, with short normal resistivity responses.

As illustrated in Figure 12, a comparison between the C1 core log and the M1 geophysical log—the two boreholes exhibiting the least karstification—demonstrates this discrepancy. In the C1 borehole, discontinuities D7 to D9 are clearly identified and supported by core observations. However, in borehole M1, the gamma-ray curve differs significantly, and only the D8bis discontinuity can be reliably identified, primarily due to the clay-rich nature of the erosional surface, which produces a clear GRN peak.

In contrast, resistivity logs provide more coherent results. For example, the D8bis discontinuity corresponds to a high-resistivity peak exceeding 3500 ohm·m, while the "Assise à terriers" Formation is characterized by a general increase in resistivity. A distinct peak around 3000 ohm·m is associated with the D7 discontinuity. These more consistent resistivity trends offer better stratigraphic correlation, although they remain locally disturbed.

The difficulty in log interpretation is partly attributed to karstic features filled with younger sediments, such as Cenomanian clays, which can significantly alter geophysical signatures (Bassil et al., 2016).

The first conductive horizon is identified on borehole M4, between 50.05 and 53.15 m depth, where a sequence of vertically stacked cavities up to 1 m in height is observed both on the OPTV log and on the long normal resistivity log (Fig. 13a). This karstified interval corresponds to a bioturbated interval that is also recognized in boreholes M09, M10, and M14. The second conductive zone, between 83 and 89 m depth, is attributed to the upper dolomitized interval. In borehole M11, a prominent cavity is located between the D7bis hardground and an overlying clay-rich horizon. This dolomitized zone, clearly delineated by low resistivity values (Fig. 13b), is consistently observed in boreholes M7, M8, and M20 (Fig. 11) and corresponds to dolomitization within the Oolitic formation.

In borehole M20, adjacent to M01, another cavity is detected from 96.4 to 102.2 m depth by acoustic data (Fig. 11). This feature lies above the D6bis discontinuity, which caps a sequence of well-preserved centimetric bioturbated strata.

Based on a long normal resistivity log, the most pronounced porous interval is the upper dolomitized zone, situated below the D7bis hardground that defines the top of the Oolitic Formation. A secondary conductive zone, above the D7 discontinuity, occurs within the Oolitic and Oncolitic formations of the *Concavum* Biozone (Aalenian) and is correlated with the middle-dolomitized zone, bounded at its base by the D7 discontinuity.

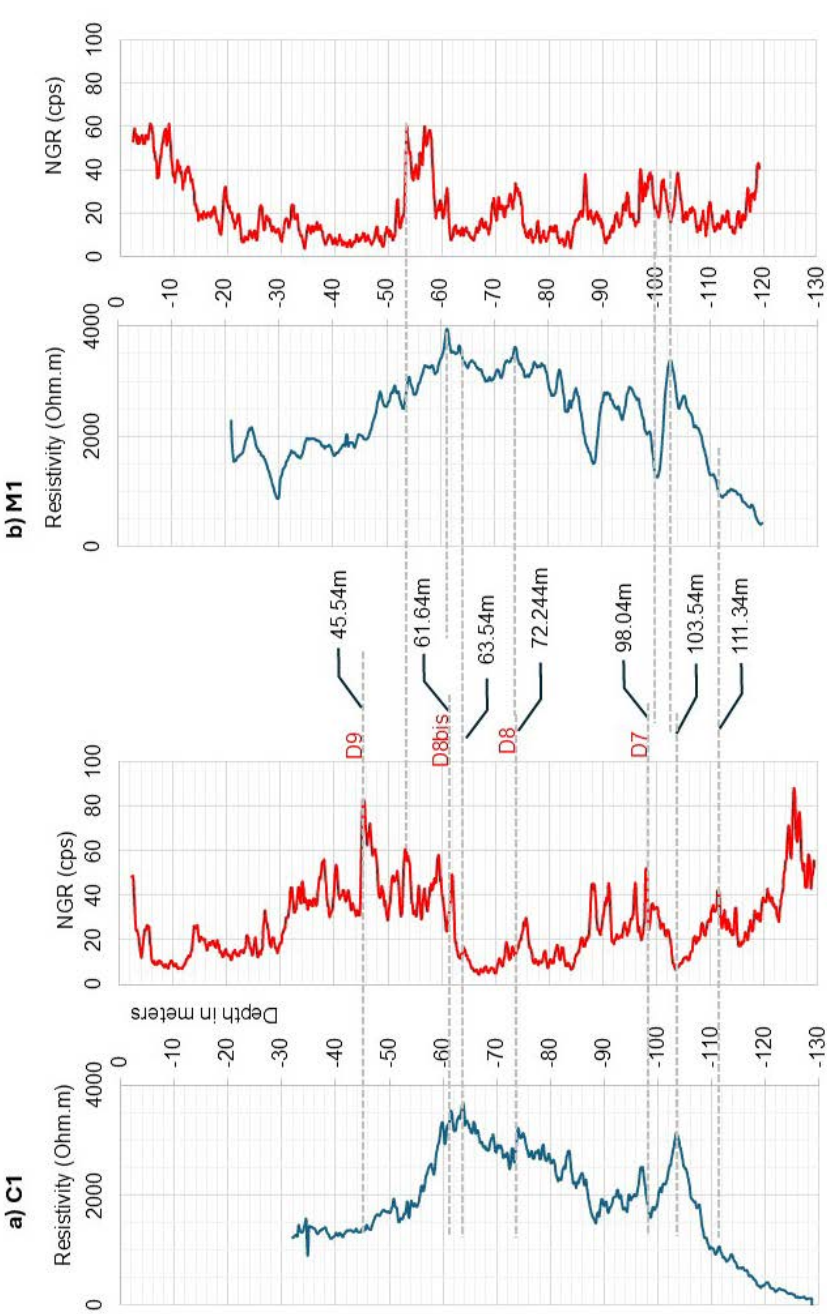

Figure 12 *Comparison of C1 and M01 logs.*

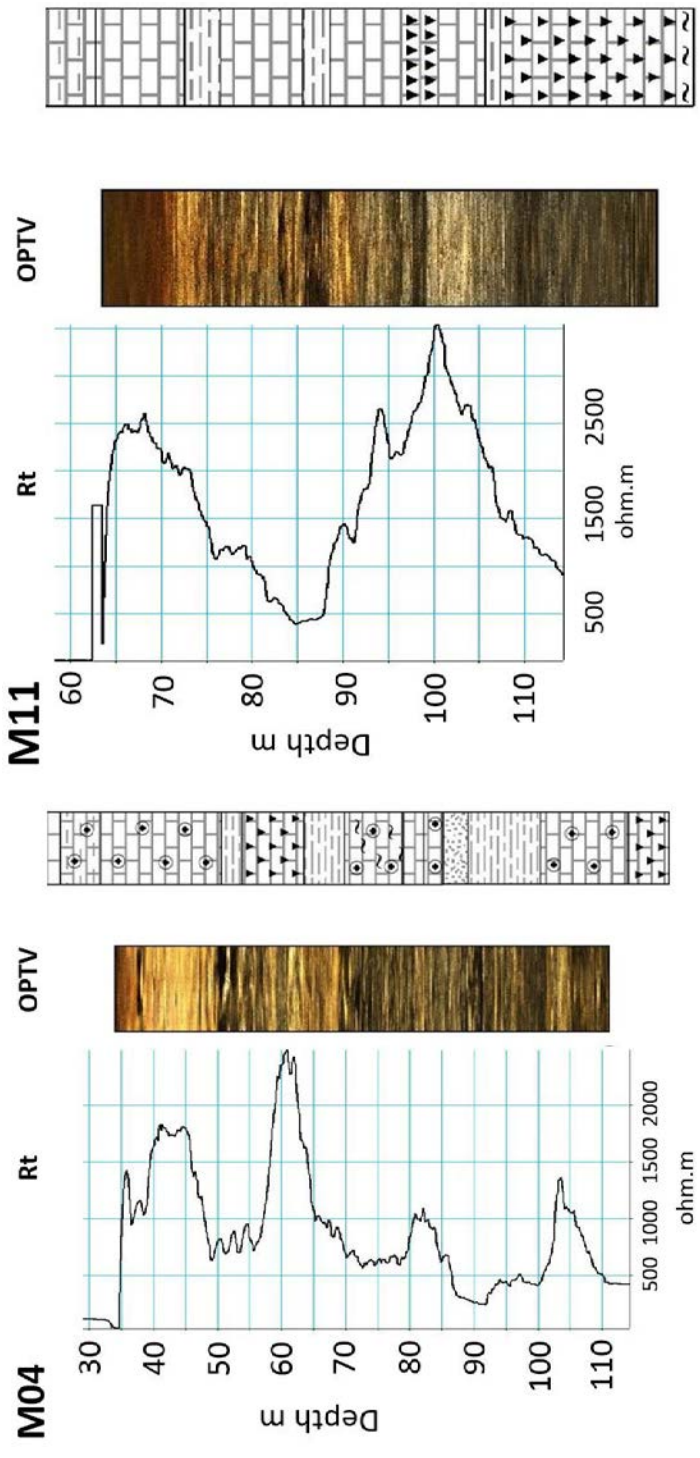

Figure 13 *Comparison of resistivity (Rt) logs and optical televiewer (OPTV) images in boreholes M04 (a) and M11 (b).*

Additionally, a marked resistivity contrast observed at ~110 m depth across all boreholes is likely associated with the D6 discontinuity and the laminated marl-limestone succession of the Opalinum Biozone (Aalenian).

In addition to conventional electrical logging, borehole electrical tests using electrical panels (Moreau et al., 2026) were conducted on the HES. Preliminary results indicate that the electrical panel sections correlate well with OPTV logs, long normal resistivity logs, and acoustic data (Mari, 2026). Electrical resistivity panels have proven to be effective in detecting individual karst conduits within the Dogger Limestone.

Stratigraphy and hydrogeological data

To complement geophysical data, flowmeter logging was conducted in selected boreholes (Audouin et al., 2008; Bodin et al., 2022; Boulais et al., 2026). These measurements aim to determine whether the porous intervals are hydraulically transmissive and capable of sustaining significant groundwater flow rates (>10 m^3/h). The goal is to assess the relationship between observed vugs and cavities and the development of an active karst system with ongoing groundwater circulation.

Audouin et al. (2008) identified an upper karstic level developed within granular limestones interbedded with cherty layers in the upper Bajocian, at a depth of approximately 50 m. This horizon is correlated with a bioturbated level situated beneath a chert bed within the *Parkinsoni* Biozone. An intermediate transmissive zone corresponds to the upper dolomitized interval of the Oolitic Formation, just below the D7bis discontinuity (at ~85 m). The lowermost productive zone, at a depth of ~110–115 m, is associated with the D6 discontinuity.

Recent hydrogeological investigations conducted by the University of Poitiers have identified productive intervals that reveal complex and spatially variable flow dynamics. Productive horizons were detected at depths of 62–65 m (MP06, M21), 72–75 m (M2, M11, M16), 80–85 m (M12, M20, M22), and 90–91 m (M11). These transmissive zones correspond to major stratigraphic discontinuities observed in boreholes, even in the absence of significant karst features (D8bis, D8, D7bis, and Upper Dolomitized Zone).

Radial convergent tracer tests further demonstrated vertical fluxes in boreholes originating from horizons at 110 m (Lower dolomitized zone), 85 m (D7bis), and 65 m (D8bis).

Flowmeter data indicate that transmissive horizons vary between boreholes, suggesting lateral discontinuity of the porous intervals and pointing to a compartmentalized aquifer structure.

Conclusion

Data acquired from various geophysical methods show a high degree of consistency and provide a coherent framework for the spatial distribution of karstic horizons identified at the Hydrogeological Experimental Site (HES) of Poitiers (France).

Importantly, fracture density alone does not account for the localization of karst features. All authors concur in describing sub-horizontal karstic levels, highlighting the predominant control of stratigraphy over structural factors. The main sedimentological controls on karst development are stratigraphic discontinuities, as described by Gabilly et al. (1985), and porous formations composed of oolitic grainstone limestones.

A synthesis of borehole optical logs (OPTV) enables the identification of distinct limestone units forming the Poitou Threshold. Through this correlation, the main karstic horizons within the supra-Toarcian aquifer are interpreted as follows:

The karst horizon at a depth of ~50 m corresponds to a bioturbated interval of the *Parkinsoni* Biozone. These beds were previously described by Benvel (1978, p. 35).

The karstic level between depths of 72 and 75 m, identified through crossflow logging, is associated with the D8 discontinuity.

The most prominent karstic horizon occurs between depths of 82 and 85 m. It lies within the Oolitic Formation. Beneath the D7bis discontinuity, the upper dolomitized zone is highly permeable.

The karstic zone observed between depths of 97 and 100 m is correlated with the D7 discontinuity. The D7 discontinuity is the upper limit of the middle-dolomitized zone contains open geodes.

The 110-115 m depth horizon is marked by D6 discontinuity and the contact with the Marl limestone lamination formation of the *Opalinum* zone. The Lower dolomitized zone began just below the D6 discontinuity.

The three dolomitized zones seem to appear under the discontinuities. The Upper one is probably related to the black clay layer, which supports pyrite and organic matter. The middle and lower zones contain centimetric microcavernes. These voids are probably the remains of fully dissolved calcite geodes.

Additional isolated cavities have been observed outside of these main discontinuities; however, they appear discontinuous and spatially limited. In the unsaturated zone, some cavities may develop along fractures in the chalky Callovian limestone, but their hydraulic connection to the main karstic horizons remains unproven. The 35 m depth horizon seems to be correlated with a bioturbated interval in the Bathonian limestone.

References

Audouin O., Bodin J., Porel G., Bourbiaux, B. (2008). Flowpath structure in a limestone aquifer: multi-borehole logging investigations at the hydrogeological experimental site of Poitiers, France. *Hydrogeology Journal*, 16 (5): 939-950. https://doi.org/10.1007/s10040-008-0275-4

Bassil J., Naveau A., Fontaine C., Grasset L., Bodin J., Porel G., Razack M., Kazpard V., Popescu S.-M. (2016). Investigation of the nature and origin of the geological matrices rich in selenium within the hydrogeological experimental site of Poitiers, France. *Comptes Rendus Geoscience*, 348 (8): 598-608. https://doi.org/10.1016/j.crte.2016.08.004

Benvel B. (1978). Étude stratigraphique, sédimentologique et structurale du Jurassique dans les vallées du Clain et de la Boivre en amont de Poitiers [Stratigraphic, sedimentological and structural study of the Jurassic in the Clain and Boivre valleys upstream from Poitiers]. Ph.D. thesis (Vol. I). Poitiers University, France.

Boulais A., Geairon H., Gaillard T. (2026). "Hydrogeological flow logging and dye tracer tests", Chapter 7 in *A new concept of karst development based on hydrogeology and geophysics*, EDP Science. https://doi.org/10.1051/978-2-7598-3934-6.c007

Bourbiaux B., Callot J.-P., Doligez B., Fleury M., Gaumet F., Guiton M., Lenormand R., Mari J.-L., Pourpak H. (2007). Multi-scale characterization of an heterogeneous aquifer through the integration of geological, geophysical and flow data: a case study. *Oil and Gas Science and Technology (IFP)*, 62: 347-373. https://doi.org/10.2516/ogst:2007029

Bodin J., Porel G., Nauleau B., Paquet D. (2022). Delineation of discrete conduit networks in karst aquifers via combined analysis of tracer tests and geophysical data. *Hydrology and Earth System Sciences*, 26 (6): 1713-1726. https://doi.org/10.5194/hess-26-1713-2022

Branger P., Gaillard T., Geairon H. (2026). "Stratigraphy of the Middle Jurassic", Chapter 2 in *A new concept of karst development based on hydrogeology and geophysics*, EDP Science. https://doi.org/10.1051/978-2-7598-3934-6.c002

Delay F., Mari J.-L., Porel G., Chabaux F., Ackerer P. (2022). Is subsurface geophysics as seismic and acoustic investigations a rescue to groundwater flow inversion? *Comptes Rendus Geoscience*, Part of Special Issue: Geo-hydrological data & models, https://doi.org/10.5802/crgeos.157

Gabilly J. (1978). *Itinéraire 12a : le versant Parisien in Guides géologiques régionaux : Poitou Charentes Vendée* [Itinerary 12a: the Parisian slope in geological guide of Poitou Charentes Vendée], with the collaboration of Brillanceau A., Cariou E., Ducloux J., Dupuis J., Hantzpergue P., Moreau P., Santallier P., Ters M., (éd. 1st edition), Masson.

Gabilly J., Cariou E., Hantzpergue P. (1985). Les grandes discontinuités du Jurassique : témoins d'évènements eustatiques, biologiques et sédimentaires [The large stratigraphic discontinuities at Jurassic time, witnesses of eustatic, biologic and sedimentary occurrences]. *Bulletin de la Société Géologique de France*, I(3): 391-401. https://doi.org/10.2113/gssgfbull.I.3.391

Gaillard T., Moreau M., Mari J.-L. (2024). Seismic and stratigraphic characterization of karstogenic horizons in a sequence of carbonate deposits: Example of the Dogger limestones of the Poitou threshold. Journées Scientifiques AGAP Qualité 2024, Poitiers, France, Edited by Asfirane, F.; Mari, J.-L.; *E3S Web of Conferences*, 504, 05005. https://doi.org/10.1051/e3sconf/202450405005

Gaillard T., Branger P. (2024). Le Jurassique moyen du seuil du Poitou [Middle Jurassic of the Poitou threshold] in *Le karst du seuil du Poitou : Approche stratigraphique et rôle de la tectonique*. Livret Guide de l'excursion du CFH sur le seuil du Poitou, 29 au 31 mars 2024.

Gaumet F., Guitton M., Callot J.-P. (2004). Hétérogénéité sédimentaire et fracturation dans le Jurassique du Site Expérimental Hydrogéologique de Poitiers [Sedimentary heterogeneity and fracturing in the Jurassic of the Hydrogeological Experimental Site of Poitiers]. Unpublished report.

Mari J.-L., Porel G. (2008). 3D Seismic Imaging of a Near-Surface Heterogeneous Aquifer: A Case Study. *Oil & Gas Science and Technology (IFP)*, 63(2): 179-201. https://doi.org/10.2516/ogst:2007077

Mari J.-L., Porel G., Bourbiaux B. (2009). From 3D Seismic to 3D Reservoir Deterministic Model Thanks to Logging Data: the Case Study of a Near Surface Heterogeneous Aquifer. *Oil & Gas Science and Technology (IFP)*, 64(2): 119-131. https://doi.org/10.2516/ogst/2008049

Mari J.-L., Porel G., Delay F. (2020). Contribution of Full Wave Acoustic Logging to the Detection and Prediction of Karstic Bodies. *Water*, 12(4): 948. https://doi.org/10.3390/w12040948

Mari J.-L., Porel G. (2024). The hydrogeological experimental site of Poitiers: Hydrogeological versus geophysical investigations, Journees Scientifiques AGAP Qualité 2024, *E3S Web of Conferences*, 504, 05003. https://doi.org/10.1051/e3sconf/202450405003

Mari J.-L. (2026). "Geophysical methods", Chapter 5 in *A new concept of karst development based on hydrogeology and geophysics*, EDP Sciences. https://doi.org/10.1051/978-2-7598-3934-6.c005

Moreau M., Brunel P., Mari J.-L. (2026). "Borehole electrical panels: an experiment", Chapter 6 *in A new concept of karst development based on hydrogeology and geophysics*, EDP Sciences. https://doi.org/10.1051/978-2-7598-3934-6.c006

Mourier J.-P. (1983). Le versant parisien du seuil du Poitou de l'Hettangien au Bathonien. Stratigraphie, sédimentologie, caractères paléontologiques, paleogéographie [The Parisian slope of the Poitou sill from the Hettangian to the Bathonian. Stratigraphy, sedimentology, paleontological features, paleogeography]. PhD thesis. Poitiers University, France.

Mourier J.-P., Gabilly J., Platel J.-P. (1986). Carte géologique de la France au 1/50000 : Notice explicative de la feuille de Poitiers [geological map of France at 1/50000 scale: Notice of Poitiers]. BRGM ed.